Electric Field Induced Selective Disordering in Lamellar Block Copolymers

Markus Ruppel,[†] Christian W. Pester,[‡] Karol M. Langner,[§] Geert J. A. Sevink,[§] Heiko G. Schoberth,[‡,#] Kristin Schmidt,[⊥] Volker S. Urban,[∥] Jimmy W. Mays,[†] and Alexander Böker[‡,*]

[†]Chemical Sciences Division, Oak Ridge National Laboratory (ORNL), Oak Ridge, Tennessee 37831, United States, [‡]DWI an der RWTH Aachen e.V., RWTH Aachen University, Aachen, NRW 52056, Germany, [§]Leiden Institute of Chemistry, Leiden University, P.O. Box 9502, 2300 RA Leiden, The Netherlands, [⊥]Stanford Synchrotron Radiation Lightsource, SLAC National Accelerator Laboratory, Menlo Park, California 94025, United States, and [∥]Biology and Soft Matter Division, Oak Ridge National Laboratory (ORNL), Oak Ridge, Tennessee 37831, United States. [#]Present address: Institute for Materials and Process Simulations, University of Bayreuth, 95440 Bayreuth, Germany.

ABSTRACT External electric fields align nanostructured block copolymers by either rotation of grains or nucleation and growth depending on how strongly the chemically distinct block copolymer components are segregated. In close vicinity to the order–disorder transition, theory and simulations suggest a third mechanism: selective disordering. We present a time-resolved small-angle X-ray scattering study that demonstrates how an electric field can indeed selectively disintegrate ill-aligned lamellae in a lyotropic block copolymer solution, while lamellae with interfaces oriented parallel to the applied field prevail. The present study adds an additional mechanism to the experimentally corroborated suite of mechanistic pathways, by which nanostructured block copolymers can align with an electric field. Our results further unveil the benefit of electric field assisted annealing for mitigating orientational disorder and topological defects in block copolymer mesophases, both in close vicinity to the order–disorder transition and well below it.

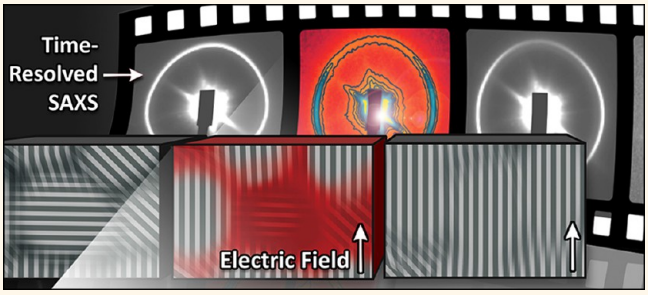

KEYWORDS: selective disordering · block copolymer · electric field · SAXS

Block copolymer self-assembly readily furnishes periodic morphologies with length scales on the order of 10–100 nm, and it is considered a powerful and cost-effective paradigm for fabricating highly ordered and densely packed nanostructures in thin films, bulk, and solutions.[1] Molecular design affords the generation of a wide variety of geometries with domain sizes below the limits of conventional optical lithography (<32 nm),[2,3] rendering block copolymer nanostructures viable components for various nanofabrication techniques.[4,5]

Using block copolymer nanostructures as templates for hierarchical pattern formation, however, demands control over long-range order and morphology. A wide range of methods have been established to this end, where chemical and physical constraints direct the self-assembly of block copolymers into highly ordered geometries. These techniques include chemically[6] and topologically patterned surfaces,[7] confined substrate geometries,[8] and external stimuli such as temperature gradients,[9] solvent annealing,[10,11] directional epitaxy,[12,13] shear,[14,15] as well as magnetic[16–19] and electric fields.[20–23]

The last option appears particularly appealing as electric fields can be applied practically instantly, localized precisely, and scale favorably with the characteristic dimensions pertaining to common nanofabrication techniques. Indeed, external fields have been successfully applied to direct the long-range order and orientation of block copolymer morphologies in thin films,[20,24–26] bulk,[27] and solution.[28] Likewise, electric fields have been demonstrated to readily control the phase behavior of low[29] and high molecular weight systems,[30–32] and to manipulate the characteristic domain

* Address correspondence to boeker@dwi.rwth-aachen.de.

Received for review September 18, 2012 and accepted April 1, 2013.

Published online April 10, 2013
10.1021/nn3059604

sizes of self-assembled block copolymers on a nanoscopic scale without the need to chemically modify the molecular architecture.[33,34] Self-assembled block copolymer nanostructures, however, often suffer from relatively high numbers of orientational and topological defects,[35] which may afflict desired material properties. Thermal annealing is commonly used to expedite the annihilation of such structural deficiencies, but alone it is often insufficient to mitigate orientational disorder on time scales relevant to common experimental and technical conditions. Moreover, processing conditions close to the order−disorder transition are notorious for propagating fluctuation-induced line and edge defects.[36−38]

Here we demonstrate how an electric field applied close to the order−disorder transition of a lamellae-forming diblock selectively disintegrates ill-aligned lamellae, while lamellae oriented parallel to the applied field prevail. Our results suggest that electric-field-assisted thermal annealing may not only stimulate the annihilation of defects in strongly segregated copolymer nanostructures, but may also diminish orientational disorder and topological defects at processing temperatures in close vicinity to the order−disorder transition.

Stability of Block Copolymer Lamellae in an Electric Field. The polarization of heterogeneous matter comprising domains of distinct dielectric permittivity in an electric field renders the free energy anisotropic.[39] As discussed by Amundson and co-workers,[27] the stationary periodic composition profile of weakly segregated block copolymers can be constructed by Fourier synthesis of sinusoidal composition waves with amplitude A and most probable wave vector $\mathbf{k}$. The excess free energy density in the presence of an external field depends on domain orientation and reads,

$$\Delta g = \frac{\beta^2}{2\bar{\varepsilon}} (\mathbf{k}\cdot\mathbf{E})^2 A^2 \qquad (1)$$

Here, $\bar{\varepsilon}$ denotes the average dielectric permittivity of the copolymer, and $\beta = \partial\varepsilon/\partial\phi$ is the local dielectric increment, which varies with the order parameter pattern $\phi(\mathbf{k})$. For simplicity, we have neglected the fact that the periodic pattern is a superposition of plane waves with various wavelengths (and amplitudes) centered about the dominant wave vector $k \equiv |\mathbf{k}|$, which in turn determines the average distance between repeating domains, $D = 2\pi/k$.

In the case of strongly segregated domains with sharp interfaces between incompatible phases, we may replace β by the macroscopic dielectric contrast between domains, *i.e.*, $\beta \rightarrow \Delta\varepsilon \equiv \varepsilon_1 - \varepsilon_2$, with ε_i denoting the dielectric permittivity of incompatible domains. In this simplified view, we implicitly neglect specific interactions between block copolymer domains and the electrode material. Furthermore, we consider only the orientation of domains far from the field source. For a thorough discussion of the effect of an electric field on dielectric interfaces in complex polymers and fluids, we refer to an excellent review by Tsori.[40]

TABLE 1. Sample Characteristics in Toluene

	$\bar{M}_n$ kg mol^{-1}	M_w/M_n	f_{PS} vol %	conc.[a] wt %	odc[b] wt %	T_{ODT} °C
$S_{42}I_{58}$ [108]	108	1.05	42	32.5	28.5	58.0 ± 0.4
$S_{48}I_{52}$ [80]	80	1.02	48	47.5	34.5	154 ± 10[c]

[a] Sample concentration. [b] Order−disorder concentration at 23 °C. [c] Approximated using $\phi^{1.6}\tilde{\chi}_t N = 14.6$ and $\tilde{\chi}_t(T) = 33.0/T - 0.0228$.[46,47]

An important implication follows from eq 1: dielectric interfaces between unlike domains that are not parallel with the field direction ($\mathbf{k}\cdot\mathbf{E} \neq 0$) are unstable; with the excess free energy density scaling as, $\Delta g \propto \Delta\varepsilon^2 E^2 \cos^2\varphi$, where φ denotes the angle between the interface normal $\hat{\mathbf{n}}$ and the applied field $\mathbf{E}$. This is the driving force that stimulates birefringent thermotropic and lyotropic block copolymer mesophases to align parallel to an applied field, and which likewise prompts electric-field-induced order−order transitions in isotropic mesophases.[31,41] As discussed by Amundson and co-workers, eq 1 further suggests that near the order−disorder transition unfavorably aligned domains with interfaces perpendicular to $\mathbf{E}$ may simply disintegrate, while those parallel to the applied field prevail.[42] Gunkel *et al.* recently sustained this assertion.[43] Predicted differences of a few millikelvin between the transition temperatures of perpendicular and parallel lamellae were, however, considered inconsequential for any practical purposes.[42]

Yet to the contrary, recent simulations by Pinna *et al.*[44] and Sevink *et al.*[45] indicate that the selective dissolution of lamellae oriented perpendicularly to an applied field may indeed be within experimental reach. We have therefore devised small-angle X-ray scattering experiments aimed to unambiguously discriminate between mechanistic pathways for the electric-field-induced alignment of block copolymer lamellae in close vicinity to the order−disorder transition.

RESULTS

We shall discuss concentrated solutions of nearly symmetric poly(styrene-*b*-isoprene) (SI) diblock copolymers (see Table 1), which readily self-assemble into a lyotropic lamellar phase at ambient temperatures with repeat distances ranging from 42 to 47 nm, depending on molecular weight and distance from the order−disorder transition (ODT). Time-resolved *in situ* small-angle X-ray scattering (SAXS) experiments were conducted employing a dedicated capacitor, which allowed precise control over the sample temperature (see Methods and Materials).

Figure 1 introduces the experimental setup. As shown, an applied field aligns lamellar planes parallel with $\mathbf{E}$. The incident beam is scattered at the lattice

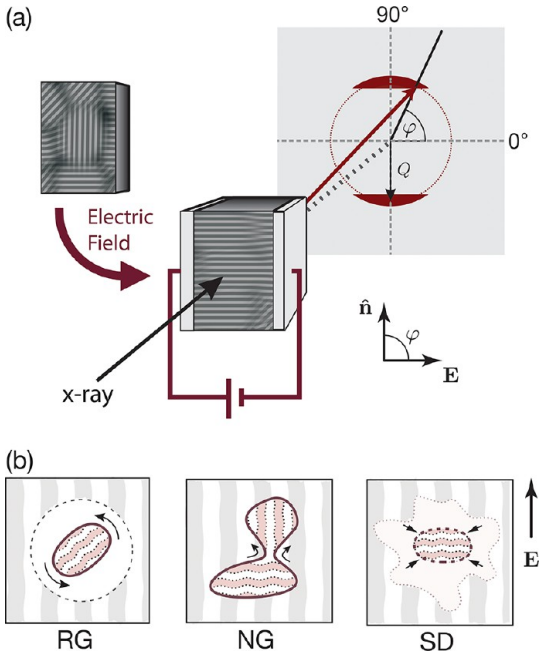

Figure 1. Experimental setup (a) and simplified cartoons illustrating possible intermediate stages for the alignment of block copolymer lamellae in the presence of an electric field E (b). Alignment of strongly segregated lamellae preferably proceeds *via* the rotation of grains (RG). Lesser segregated diblock lamellae preferentially align through nucleation and growth (NG). Here, critical layer undulations nucleate the formation of new grains; lamellar planes of which are aligned parallel to the applied field. NG proceeds through continuous grain boundary migration during the early and intermediate stages. In proximity to ODT, and thus in the limit of weak segregation, alignment may proceed through the selective disintegration of lamellar grains (SD). Apparent alignment then proceeds through the coarsening of nearby parallel lamellae and/or the nucleation of new grains from the disordered melt. φ designates the angle between the lamellar normal n̂ and the applied field, which coincides with the dominant azimuthal scattering angle for finite orientational order. Lamellar planes are aligned parallel with E for $\varphi = 90°$. Q denotes the scattering wave vector, which is related to the radial scattering angle θ by, $Q = 4\pi/\lambda \sin\theta$, where λ is the wavelength of the incident beam.

planes and thus along the lamellar normal $\hat{\mathbf{n}}$. In what follows, φ denotes the angle between **E** and $\hat{\mathbf{n}}$. As such, φ coincides with the azimuthal scattering angle, which indicates the mean orientation of lamellar planes. The structure of lamellae with particular orientation can thus be selectively assessed by analyzing the radial intensity distribution; azimuthally averaged within wedged-shaped sectors of chosen orientation.

Mechanisms of Alignment. The alignment of lamellae in the presence of an electric field may proceed *via* either of the following mechanistic pathways (see Figure 1): rotation of grains (RG), nucleation and growth (NG), or selective disordering (SD). Field-induced rotation of grains is the dominant mechanism in strongly segregated block copolymers or in situations where lamellae are already close to their preferred orientation.[48,49] Nucleation and growth is the prevalent mechanism for systems of intermediate segregation. The mechanism is distinct as compared to the nucleation and growth in an isotropic liquid insofar as NG proceeds through continuous grain boundary migration, sustained by the presence of ill-aligned lamellae. Selective disordering identifies the situation when ill-aligned lamellar grains selectively dissolve to yield a disordered melt, while proper aligned lamellae prevail. SD is predicated on differences of the order−disorder transition temperature (T_{ODT}) depending on lamellar orientation ($\delta T_{ODT}(\varphi) \sim \cos^2 \varphi$). Those differences are due to the polarization of interfaces, which are inhomogeneous with **E**.[43] Early on, SD was proposed to be a viable path for lamellar alignment in close vicinity to ODT, and thus in the limit of weak segregation.[42] Lamellar alignment may then proceed through either the coarsening of existing (well-aligned) lamellae and/or the nucleation of new lamellar grains from the disordered melt. The process of selective disordering of ill-aligned lamellae in the presence of an electric field is on the focus of the present study. A detailed analysis of the orientation dependent shift of $T_{ODT}(\varphi)$ will be discussed in a subsequent communication.[50]

Rotation of Grains and Nucleation and Growth. To prudently assess our experimental observations in close vicinity to ODT and to provide some guidance as regards the characteristic evolution of the scattering patterns pertaining to RG and NG, we start by briefly reiterating previously published SAXS data of the field-induced alignment of a lyotropic lamellar solution of $S_{48}I_{52}$[80] in toluene (47.5 wt %).[48] Figure 2 highlights the scattering properties discerning between RG (left), which is the relevant mechanism for strongly segregated $S_{48}I_{52}$[80] at 27 °C, and NG (right), which dominates the alignment for intermediate segregation closer to ODT at 80 °C.

Representative time series of 2D scattering data for both scenarios are shown in Figure 2a. In the absence of an applied field (images to the left, $t = 0$ s), lamellar planes are initially typically oriented parallel to the electrodes, owing to shear stress upon filling the capacitors.[49] Accordingly, the scattering intensity accumulates in the vertical direction, highlighted by a wedge-shaped sector at $\varphi = 0°$. We note that the field is applied horizontally in laboratory coordinates as depicted in Figure 1a, yet the detector plane was rotated by 90°. First- and second-order Debye−Scherrer rings at relative ratios (Q_{hkl}:Q_{100} = 1:2) indicate the lamellar morphology. Upon inception of the field, lamellar planes align parallel with **E** and the scattering intensity eventually accumulates in horizontal sectors denoted by $\varphi = 90°$ (images to the right).

The essential differences between RG and NG become apparent from the time evolution of the azimuthal scattering intensity in Figure 2b (integrated about the location of the primary Bragg-peak Q_{max}). Gradual grain orientation, as being distinctive for RG,

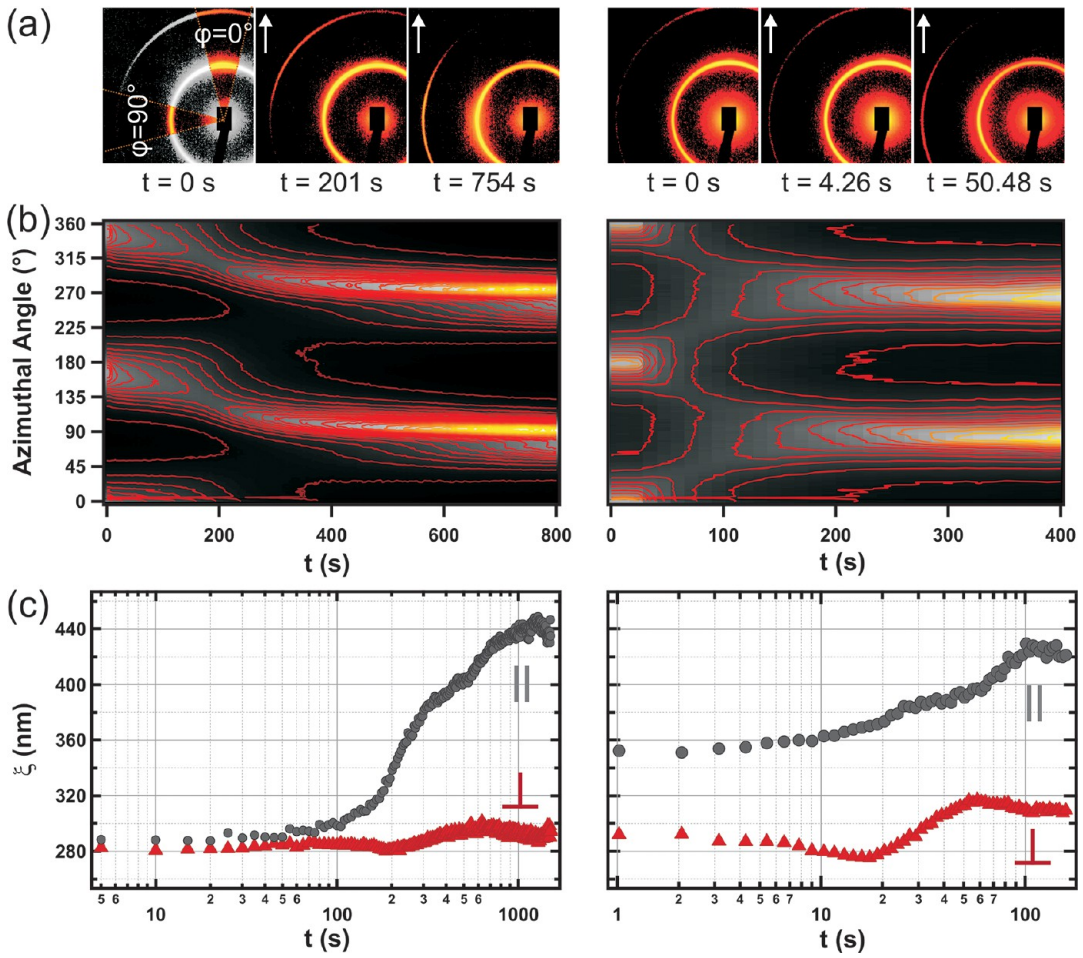

Figure 2. 2D small-angle X-ray scattering patterns (a) and azimuthal intensity distribution of the primary Bragg-peak located at $Q_{max} = 0.15 \pm 0.017$ nm^{-1} (b) after inception of an electric field of 1 kV mm^{-1} for a concentrated lamellar solution of $S_{48}I_{52}$[80] in toluene (47.5 wt %). The CCD-image to the upper left demonstrates the sector geometry used for computing the azimuthally averaged sector intensities. The sectors at azimuthal angles $\varphi = 90 \pm 15°$ and $\varphi = 0 \pm 15°$ correspond to lamellae oriented parallel and perpendicularly to E, respectively. The white arrows indicate the direction of the applied field. The time evolution of the azimuthal location of the primary Bragg-peak documents grain rotation (GR) and nucleation and growth (NG) as the prevalent mechanisms at $T = 27$ °C (left) and $T = 80$ °C (right), respectively.[48] The corresponding time evolution of the correlation length ξ, for parallel (black circles) and perpendicular (red triangles) lamellae, is shown in panel c.

becomes evident through the presence of a continuous intensity trace spreading over intermediate azimuthal angles. Such a distinct trace is absent for NG and lamellae with interfaces parallel to **E** ($\varphi = 90°$) simply grow at the expense of perpendicular ones ($\varphi = 0°$). Both mechanisms, and their dependence on the degree of phase separation, are well established and corroborated by experiments,[42,49,51] computer simulations[44] and theory.[52]

Transverse Grain Size and the Correlation Length. For this study, we reexamined the data presented in Figure 2 to obtain information about the transverse lamellar grain dimension, that is, the dimension *perpendicular* to the lamellar interface. The structural changes pertinent to lamellae aligned parallel and perpendicular to **E** were analyzed independently by computing the radial scattering distributions (azimuthally averaged intensity as a function of scattering vector Q) within wedge-shaped sectors at azimuthal angles $\varphi = (0 \pm 15)°$ and $\varphi = (90 \pm 15)°$. The radial data is shown in Figure 2a (left). The repeat distance between lamellar domains is given by the location of the primary Bragg-peak at Q_{max} as, $D = 2\pi/Q_{max}$. The transverse grain dimension can be envisaged as the average length scale over which chemically homogeneous domains are correlated. As such, it measures the degree of translational order and follows naturally from the breadth of the primary peak intensity. The peak width is largely determined by grain size. However, peak broadening occurs owing to layer dislocations, topological defects, and paracrystalline disorder.[53,54] All of which abate apparent translational order. Using a Pseudo-Voigt line shape analysis, the width was taken as the full-width at half-maximum (fwhm) and the correlation length was computed as $\xi = 2/\text{fwhm}$. Considering a synchrotron X-ray small-angle scattering geometry, instrument broadening was negligible (*cf.* Methods and Materials).

The time evolution of ξ after turning on the electric field is shown in Figure 2c for both RG and NG. The degree of domain segregation was controlled by temperature. At ambient conditions (T = 23 °C), lamellar alignment proceeds *via* RG (Figure 2c, left), and the correlation lengths of lamellae initially oriented perpendicularly ($\xi_\perp$) and parallel ($\xi_\parallel$) to **E** barely change during the initial stage. Once significant amounts of lamellae start to rotate toward the field ($t \geq$ 50 s), $\xi_\parallel$ significantly increases by about 50%. In contrast, $\xi_\perp$ remains virtually unchanged, supporting the notion that RG proceeds through the migration and annihilation of defects perpendicular to **E**. Defect annihilation also enables the coarsening of parallel-aligned lamellae in an applied field.[42] Yet, a minor fraction of ill-aligned lamellae may persist, and their thermal coarsening is indicated by a slight increase in $\xi_\perp$ during intermediate stages.

At a higher temperature (T = 80 °C), and thus for lessened diblock segregation, alignment proceeds *via* NG (Figure 2c, right). Noteworthy is the initial drop of $\xi_\perp$, which onsets the slow but steady growth of $\xi_\parallel$ parallel to **E**. We attribute the initial decline of $\xi_\perp$ to the key phenomenon responsible for NG: electric-field-induced in-plane undulations or buckling layer instabilities first proposed by Onuki,[52,55] and reminiscent of Helfrich-Hurault instabilities in smectics in magnetic and shear fields.[56] In the presence of an electric field, in-plane undulations grow in amplitude and become unstable above a critical field strength E^*, which scales with lamellar dimension as $E^* \sim \xi^{-1/2}$.[52,57] Here, we have neglected some minor deviations from the square-root scaling, when the transverse grain size approaches the repeat distance between lamellar stacks.[58] The notion of a critical field implies the existence of a critical grain size $\xi_\perp^*$, for which perpendicularly aligned lamellae become unstable and nucleation of parallel lamellae ensues. Their growth and coarsening eventually lead to a lamellar morphology, predominantly aligned parallel to **E**. Indeed, it is evident from Figure 2b (right) that a gradual increase in $\xi_\parallel$ coincides with the initial drop of $\xi_\perp$.

The recovery of $\xi_\perp$ during the intermediate stages of NG deserves a comment. Perpendicular lamellae with $\xi_\perp < \xi_\perp^*$ are stable against undulations, yet they are susceptible to thermal and electric-field-induced coarsening. Once the grain size exceeds $\xi_\perp^*$, ill-aligned lamellae become unstable and spawn the formation of parallel lamellae. We thus anticipate that the time evolution of $\xi_\perp$ is determined by a subtle balance between coarsening and the induction of in-plane undulations for $\xi_\perp > \xi_\perp^*$. Figure 2b indeed indicates such an asymptotic convergence of $\xi_\perp$ during the later stages.

Situation for Weak Segregation. We now turn to the situation in close vicinity to ODT. Here, the alignment of block copolymer lamellae was recently predicted to proceed *via* selective disordering, that is, ill-aligned lamellae disintegrate and the resulting melt allows parallel lamellae to grow.[44,45] We thus studied the alignment of a lamellar phase in proximity to T_{ODT} within a small window below ODT, for which $|T - T_{ODT}| \leq$ 2.6 K. In the remainder of this article we will denote the distance from ODT by $\Delta T \equiv T - T_{ODT}$, where T is the sample temperature.

We used a lyotropic solution of $S_{42}I_{58}$[108] in toluene (32.5 wt %), whose transition temperature was determined as T_{ODT} = 58.05 ± 0.43 °C. This translates to a bulk (solvent-free) value for the thermodynamic segregation strength at the transition of $\phi^{1.6}\tilde{\chi}_t N \approx 14.8$. Here, we applied the modified dilution approximation for semidilute solutions of block copolymers in a neutral solvent,[46,47] where ϕ accounts for the polymer's volume fraction, $\tilde{\chi}_t$ is the fluctuation-corrected interaction parameter at the transition, and N is the number of copolymer segments. As mentioned above, a preferred orientation is generally noticeable prior to the application of any field. This is usually attributable to shear stress upon filling the capacitors. Care was thus taken to equilibrate the samples well above ODT to ensure an isotropic distribution of lamellae below ODT prior to the application of the electric field. Still, we noticed a minor bias of lamellae to preferably aligned perpendicular to the electrodes when cooled below ODT. This may be due to a gravitational effect, which biases lamellar stacks to settle horizontally and leads to an initial anisotropy in both $I_{max}(t = 0\ s)$ and $\xi(t = 0\ s)$ as being evident throughout this study.

Figure 3a shows azimuthally averaged SAXS data for sectors corresponding to lamellae parallel (red solid line) and perpendicular to **E** (black broken line), both for a sample farther below ODT ($\Delta T = -2.6$ K), 10 s after inception of an external field of 1, and for a sample closer to ODT ($\Delta T = -1.0$ K), 5 s after turning on the field. In both cases, $I_{max}^\perp$ peak intensities are substantially lower, a mere consequence of the diminishing volume fraction of perpendicular lamellae when aligned parallel to **E**.

Far more conclusive is the time evolution of the peak width. In close vicinity to ODT ($\Delta T = -1.0$ K), the decreasing peak scattering intensity $I_{max}^\perp$ is accompanied by a considerable change in peak width; the peak becomes broad and adopts a near-ideal Lorentzian line shape (*cf.* Supporting Information and Figure S1 therein). The distinct broadening of the primary peak indicates the transition from an ordered to a disordered (liquid-like) state.[59−62] Considering that spatial composition fluctuations of block copolymers are confined about the dominant wave vector Q_{max}, the scattering intensity above ODT can then be approximated by $I(Q) \simeq I(Q_{max})/[1 - \xi^2(Q - Q_{max})^2]$,[63,64] which identifies a Lorentzian with ξ = 2/fwhm. In the disordered state, the correlation length thus represents the average length scale over which composition fluctuations are coherent.

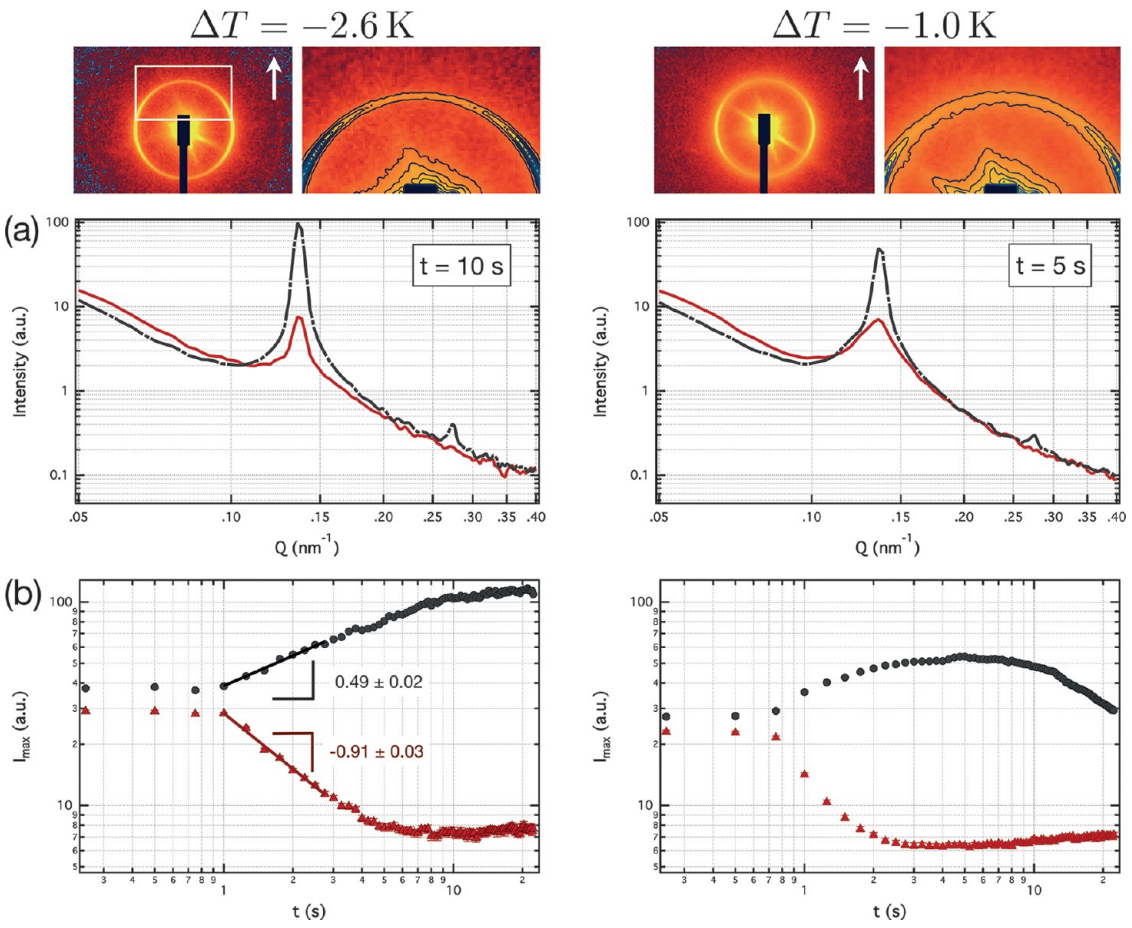

Figure 3. Azimuthally averaged X-ray scattering intensity as a function of wave vector *Q* (a), and time evolution of the peak intensity I_{max} (b) after inception of an electric field, $E = 1$ kV mm^{-1}, for a concentrated solution of $S_{42}I_{58}$[108] (32.5 wt %) at $T = 55.5$ °C (left) and $T = 57.1$ °C (right). Representative azimuthally averaged intensity data are shown for both parallel (black broken line) and perpendicularly aligned lamellae (red solid line). Depicted data were recorded at $t = 10$ s and $t = 5$ s after inception of E. The top row displays the corresponding 2D scattering images, including magnifications at the right highlighting regions governed primarily by perpendicular aligned lamellae (dark lines indicate iso-intensity contour levels). The time evolution of the peak intensity is shown for lamellae parallel (black circles) and perpendicular (red triangles) to E (b). Here, the solid lines represent power law fits to the experimental data recorded at $T = 55.5$ °C. An apparent scaling $I(q) \sim t^{\alpha}$, with $\alpha = 0.49 \pm 0.02$ and $\alpha = -0.91 \pm 0.03$, was found for parallel and perpendicular lamellae, respectively. The distance from ODT is indicated by $\Delta T = T - T_{ODT}$, with $T_{ODT} = 58.0 \pm 0.4$ °C in the absence of an applied field. White arrows indicate the direction of E. Identical intensity scaling is retained for all scattering images shown.

We further note that scattering patterns emanating from parallel aligned lamellae generally sustain a well-defined secondary Bragg-peak (see Figure 3a). This is noteworthy as layer undulations (thermal and field-induced) naturally impair the positional order of lamellar planes. Indeed, strain broadening increases linearly with harmonic number[54] and strong undulations may readily suppress Bragg-peaks of higher order. This is particularly true for lyotropic phases close to ODT, where thermal fluctuations render the degree of positional order merely quasi-long ranged[65] (as opposed to well-defined positional order found in strongly segregated lamellar phases well below ODT or in bulk). An electric field applied in in-plane direction, however, stabilizes lamellar planes, making them less susceptible to long-wavelength undulations.[43,52] As outlined above, the opposite is true for perpendicularly aligned lamellae, where an applied field above E^* triggers the divergence of layer undulations.

The time evolution of I_{max} after inception of E is depicted in Figure 3b. It highlights the increase of the volume fraction of parallel lamellae at the expense of the perpendicular population irrespective of ΔT. It is worth noting that for $\Delta T = -2.6$ K, the early time evolution of the peak intensity for parallel ($I^{\parallel}_{max}$) and perpendicular ($I^{\perp}_{max}$) lamellae follows the apparent scalings $I^{\parallel}_{max} \sim t^{\alpha}$ and $I^{\perp}_{max} \sim t^{-2\alpha}$, respectively, with $\alpha \approx 0.5$. This is in good agreement with predictions by Onuki and Fukuda[52] for NG, when the growth of parallel lamellae is governed by hydrodynamic interactions. Indeed, the time evolution of I_{max} for samples of $S_{48}I_{52}$[80], whose alignment proceeds *via* NG at $T = 80$ °C (*vide supra*), likewise revealed comparable scaling exponents (see Supporting Information, Figure S4). It also deserves mentioning that we observed a decline

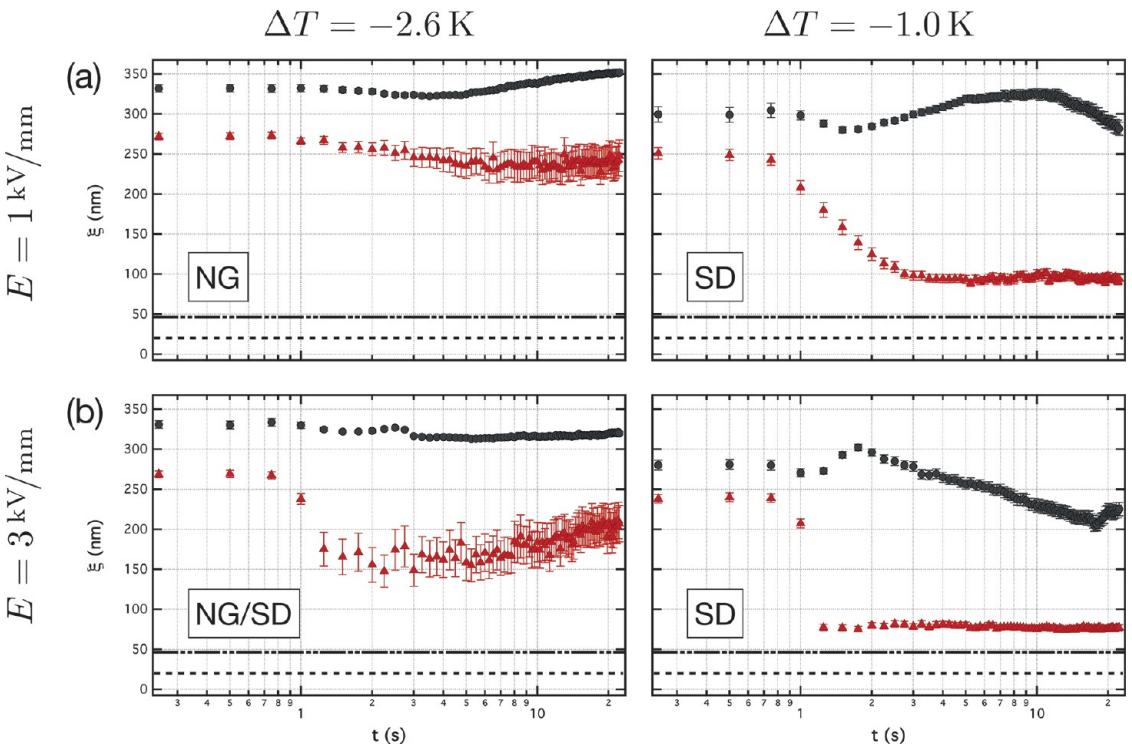

Figure 4. Time evolution of the correlation length ξ for a concentrated solution of $S_{42}I_{58}$[108] in toluene (32.5 wt %) at $T = 55.5$ °C (left) and $T = 57.1$ °C (right). The time-resolved data demonstrate the evolution of ξ for lamellae oriented perpendicularly (dark red triangles) and parallel (dark gray circles) to E, for $E = 1$ kV mm^{-1} (a) and $E = 3$ kV mm^{-1} (b). The data illustrates the time evolution of ξ for nucleation and growth (NG), selective disordering (SD), and an intermediate regime, where both mechanisms coexist (NG/SD). The dashed and dotted horizontal lines indicate the lamellar repeat distance, $D = 47.5$ nm, and the size of the unperturbed diblock, $2R_g = 20$ nm. $\Delta T = T - T_{ODT}$ indicates the distance from ODT.

in $I^{\parallel}_{max}$ during the very late stages after inception of E for samples studied very close to ODT, that is, the volume fraction and/or the size of parallel aligned lamellae decreases. We attribute this to mere thermal equilibration, which causes grains of parallel-aligned lamellae to attain an equilibrium size as supported by an equal decline in $\xi_{\parallel}$. Note that an applied field slightly stabilizes the disordered phase independently of lamellar orientation.[30,32] Hence, the equilibrium size of lamellar grains in the presence of an applied field is well anticipated to be somewhat smaller than in the absence of an electric field (*vide infra*).

Selective Disordering. Figure 4 compiles the time evolution of ξ upon inception of an applied field in proximity to ODT. Here, we focus on the situations for both $\Delta T = -1.0$ K and $\Delta T = -2.6$ K at a lower and higher field strength, namely $E = 1$ kV mm^{-1} (a) and $E = 3$ kV mm^{-1} (b). Even for a relatively low field, there is a marked difference in the response of parallel and perpendicular lamellae. While both, $\xi_{\parallel}$ and $\xi_{\perp}$, barely change for $\Delta T = -2.6$ K, the correlation length of perpendicularly aligned lamellae significantly drops in close vicinity to ODT, namely, $\Delta T = -1.0$ K. Here, $\xi_{\perp}$ asymptotically approaches the lamellar repeat distance ($D = 47.5$ nm), that is, the correlations between identical phases barely extend over two lamellar stacks in the later stages ($\xi_{\perp} \approx 100$ nm). In contrast, $\xi_{\parallel}$ increases during intermediate stages, irrespective of ΔT, following a decline during the early stages. Thus, for $\Delta T = -2.6$ K, well-defined lamellae persist irrespective of initial orientation, while perpendicular lamellae substantially disintegrate in close vicinity to ODT.

At a higher field strength ($E = 3$ kV mm^{-1}), lamellar disintegration is evident even farther below ODT (*i.e.*, $\Delta T = -2.6$ K). For $\Delta T = -1.0$ K, $\xi_{\perp}$ declines to just about 1.7 times the value of the initial lamellar repeat distance, which amounts to about four times the bulk size of a single diblock ($2R_g = 20$ nm). Yet, $\xi_{\parallel}$ sustains a significantly larger magnitude ($\xi_{\parallel} > 200$ nm) even at high field intensities and in close vicinity to ODT. This is in stark contrast to lamellae initially aligned perpendicularly to **E**, which disintegrate almost entirely and exhibit transverse dimensions typical for correlated composition fluctuations in the disordered phase.[60,61,66]

We shall also comment on the time evolution of $\xi_{\parallel}$ in close vicinity to ODT ($\Delta T = -1.0$ K). $\xi_{\parallel}$ barely changes at first, but later increases and subsequently declines. We may readily account for this behavior when we appreciate ξ as an ensemble average. The disintegration of perpendicular lamellae upon inception of the field enables the formation of new grains, with planes aligned parallel with **E**. Pristine grains will naturally exhibit smaller dimensions at first, compared to the matured population, and $\xi_{\parallel}$ will consequently be lower

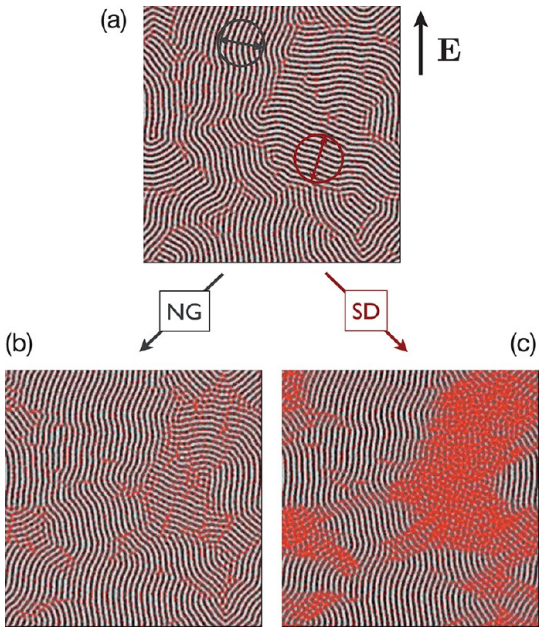

Figure 5. DDFT simulation data of a lamellar diblock morphology in close vicinity to ODT upon inception of an electric field. In the absence of an applied field, lamellae are randomly distributed (a). The embedded pictograms illustrate the transverse correlation length 2ξ for lamellae oriented parallel (black) and perpendicularly (red) to E. In the presence of a strong electric field (dimensionless field strength $\tilde{\alpha} = 0.1$ as explained elsewhere[45]) perpendicularly aligned lamellae selectively disintegrate (b, red shaded areas), corroborating the same selective disordering (SD) demonstrated experimentally. At lower fields ($\tilde{\alpha} = 0.02$), lamellar alignment proceeds *via* NG, that is, ill-aligned lamellae become unstable against buckling layer instabilities, which nucleate the growth of parallel aligned lamellae (c). Movies illustrating the time-resolved process in real space for both NG and SD are provided as Supporting Information.

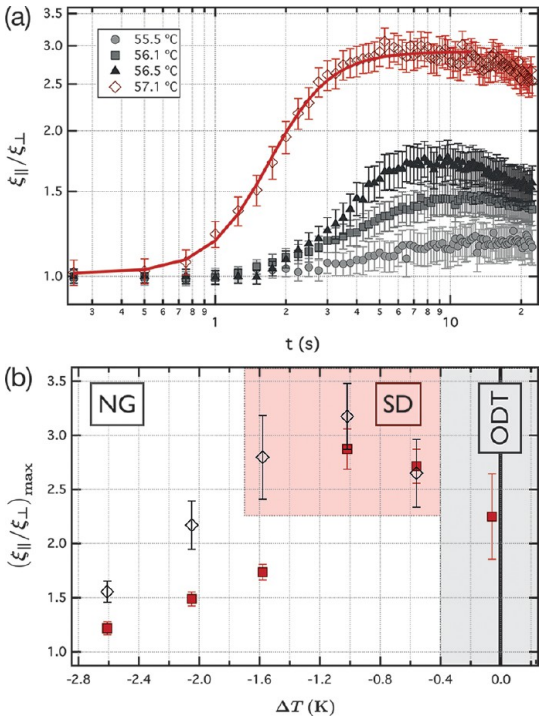

Figure 6. Time evolution of the normalized correlation length asymmetry ($\xi_\parallel/\xi_\perp$) upon inception of an electric field, $E = 3$ kV mm^{-1} (a). A sigmoidal function was fitted to the experimental data to gauge the asymptotic behavior for $t \to \infty$ (solid red line), yielding a plateau value $(\xi_\parallel/\xi_\perp)_{max}$ that measures the highest anisotropy in ξ. For the sake of clarity, the data for $T = 57.6$ °C and $T = 58.0$ °C are omitted (see Figure S3 in Supporting Information) and the ratio $\xi_\parallel/\xi_\perp$ was normalized by its initial value at $t = 0$. The transition from nucleation and growth (NG) to selective disordering (SD) can be delineated by $(\xi_\parallel/\xi_\perp)_{max}$ as a function of ΔT (b). Data are shown for an applied field of 1 kV mm^{-1} (solid red squares) and 3 kV mm^{-1} (open black diamonds). The solid black vertical line designates $T_{ODT} = 58.0$ °C in the absence of an external field and the gray shaded area highlights the experimental width for T_{ODT} (±0.4 °C), where nonselective disordering is dominant.

in the early stages. The intermediate increase of $\xi_\parallel$ then follows naturally considering the growth of pristine grains and concurrent electric-field-induced coarsening of existing parallel lamellae.[67] Nonetheless, the kinetically controlled intermediate grain size is likely not the equilibrium size, which is determined by both ΔT and the field strength. Since an external field stabilizes the disordered phase and thus shifts T_{ODT} somewhat downward,[32] we attribute the decrease in $\xi_\parallel$ during the later stages to thermal equilibration alone (*vide supra*) .

DDFT Simulations: Situation in Real Space. Figure 5 complements our experimental results with real space snapshots obtained from dynamic density-functional theory (DDFT) simulations in the ordered phase in proximity to ODT ($\chi_t N = 14.7$). Prior to applying an electric field, the diblock morphology comprises randomly oriented lamellae (Figure 5a). In accordance with the experimental data, subsequent reorientation proceeds in a way that depends on field strength—*via* NG at low fields and through SD at higher fields. For selective disordering in particular, lamellae initially oriented perpendicularly to **E** selectively disintegrate leaving disordered regions (Figure 5b, red shaded areas), whereas parallel aligned lamellae remain unaffected. When alignment proceeds *via* NG, perpendicular lamellae become unstable and undulations nucleate the formation of parallel aligned lamellae as indicated in Figure 5c. Movies illustrating the lamellar alignment through NG and SD in real space are provided as Supporting Information (Figure S2). For details concerning the simulation method and electric field parametrization, we refer to a previously published report.[45]

Transition from NG to SD. In an attempt to quantify the degree of selective disordering for various temperatures close to ODT, we evaluated the time evolution of the correlation length asymmetry $\xi_\parallel/\xi_\perp$. Depicted in Figure 6a, $\xi_\parallel/\xi_\perp$ discriminates between an isotropic and anisotropic response of ξ in the presence of a field, and consequently approaches unity in the limit of a purely isotropic response. This is indeed the case for nonselective disordering being evident for sample

temperatures nearest to T_{ODT} and/or at a high field strength. We reiterate the field-induced downward shift of T_{ODT} for SI,[32] which eases nonselective melting even farther away from $T_{ODT}(E = 0)$ (see Supporting Information, Figure S3). In the case of selective disordering, however, $\xi_{\parallel}/\xi_{\perp}$ generally follows a sigmoidal path and approaches a plateau. Close to ODT, where lamellar alignment may proceed either *via* NG or SD, we used the upper asymptotic limit $(\xi_{\parallel}/\xi_{\perp})_{max}$ to probe the strength of the anisotropic response, while also accounting for experimental errors.

Figure 6b summarizes the temperature dependence of $(\xi_{\parallel}/\xi_{\perp})_{max}$ for applied fields of both 1 kV mm^{-1} (red solid squares) and 3 kV mm^{-1} (open diamonds). $(\xi_{\parallel}/\xi_{\perp})_{max}$ generally increases with temperature, approaches a maximum and then decreases in close vicinity to T_{ODT}, where nonselective disordering becomes prevalent for $\Delta T_{ODT} \geq -0.5$ K. Quantitatively, this agrees well with the observed stabilization of the disordered phase in the presence of an electric field as reported previously.[32] For lower temperatures, however, we notice a distinct increase of $(\xi_{\parallel}/\xi_{\perp})_{max}$ for $E = 1$ kV mm^{-1} at $\Delta T = -1.0$ K. Considering the substantial suppression of $\xi_{\perp}$ as outlined above (*cf.* Figure 4b), we discern the transition where SD becomes the dominant mechanism at $\Delta T = -1.0$ K, accordingly. For $E = 3$ kV mm^{-1}, we generally obtain higher absolute values for $(\xi_{\parallel}/\xi_{\perp})_{max}$ at lower temperatures as well as a more continuous transition. When compared to the lower field data, SD becomes the dominant mechanism at $\Delta T = -1.6$ K. The asymptotic limit $(\xi_{\parallel}/\xi_{\perp})_{max}$ thus demarcates a narrow window in proximity to ODT (red shaded area in Figure 6b), where selective disordering exists as the prevailing mechanism.

SUMMARY AND DISCUSSION

When Amundson and co-workers discussed the viable mechanistic pathways for the electric-field-induced alignment of block copolymer mesophases,[42] they critically remarked on the fact that eq 1 adds an orientation dependent term to the free energy, which renders the controlling combination $\tilde{\chi}N$ anisotropic. By renormalizing $\tilde{\chi}N$ to account for electrostatic contributions in the presence of an electric field, the orientation dependent electrostatic excess term was treated akin to an elastic contribution due to mechanic deformations of copolymer lamellae. By doing so, they estimated a shift, $\Delta T_{ODT} \equiv T_{ODT}^{\perp} - T_{ODT}^{\parallel}$, of barely a few millikelvins for a poly(styrene-*b*-methyl methacrylate) diblock (SM) exposed to a field of 1.8 kV mm^{-1}.[42] While SM exhibits a significant dielectric contrast between its chemically distinct components ($\Delta\varepsilon = 1.23$), SI diblocks, as discussed in the present study, provide a considerably weaker contrast (*i.e.*, $\Delta\varepsilon = 0.2$; with $\varepsilon(S) = 2.6$ and $\varepsilon(I) = 2.4$) and no significant difference between the transition temperatures of orthogonally oriented lamellae was anticipated.

Selective Disordering: A Viable Mechanism? Recent simulations by Pinna *et al.*[44] and Sevink *et al.*,[45] suggest that SD may in fact be of experimental significance close to ODT within a much wider window than previously thought. Indeed, early time-resolved studies by DeRouchey and co-workers well below ODT ($\Delta T = -137$ K) hinted at the transient dissolution of initially perpendicularly aligned lamellae during the electric-field-induced alignment of diblock lamellae in thin films.[68] Azimuthally averaged SAXS data exhibited a distinct broadening of the dominant peak at Q_{max}. However, the scattering geometry they employed allowed them to probe only the evolution of lamellar grains averaged over all orientations within $45° \leq \varphi \leq 90°$. This means that the observed line broadening may have resulted from a heterogeneous distribution of lamellar orientations with varying periodicity, and possibly exaggerated by a broad distribution of grain sizes, rather than from a distinct disintegration of lamellar grains (the latter explicitly entails diminished long-range order between coherent phases).

In this study, we focused on the time evolution of the transverse correlation length ξ in order to validate the existence of selective disordering. Below ODT, ξ directly determines the transverse grain dimension, while in the disordered state ξ represents the length scale over which evanescent composition modulations are correlated. More importantly, our scattering geometry allowed us to independently assess the behavior of perpendicularly and parallel aligned lamellae.

Upon inception of an external field, we observed a substantial anisotropic response of ξ depending on the initial lamellar orientation. In the case of perpendicular lamellae close to ODT, $\xi_{\perp}$ considerably declined, while $\xi_{\parallel}$ remained mostly unperturbed (see Figure 4a). According to $\xi = 2/\text{fwhm}$, the decrease in $\xi_{\perp}$ marks a substantial broadening of the peak shape at Q_{max}—a distinct change commonly observed upon disordering at ODT.[61,69,70] Indeed, in close vicinity to ODT ($\Delta T = -1.0$ K), $\xi_{\perp}$ indicated transverse dimensions of barely twice the lamellar repeat distance ($D = 47.5$ nm). We thus consider $\xi_{\perp}$ to be predominately governed by nonstationary composition modulations, which determine the structure in the disordered phase close to the transition. The situation was even more explicit at a higher field strength (see Figure 4b). We thus conclude that SD can indeed be experimentally attested within a narrow window in close vicinity to ODT. Our experimental data are well corroborated by DDFT simulations, which demonstrate the selective disordering of ill-aligned lamellae in proximity to ODT in real space (*cf.* Figure 5 and movies in Supporting Information, Figure S2).

In an attempt to quantify the degree of selective disordering as a function of ΔT, and to demarcate the

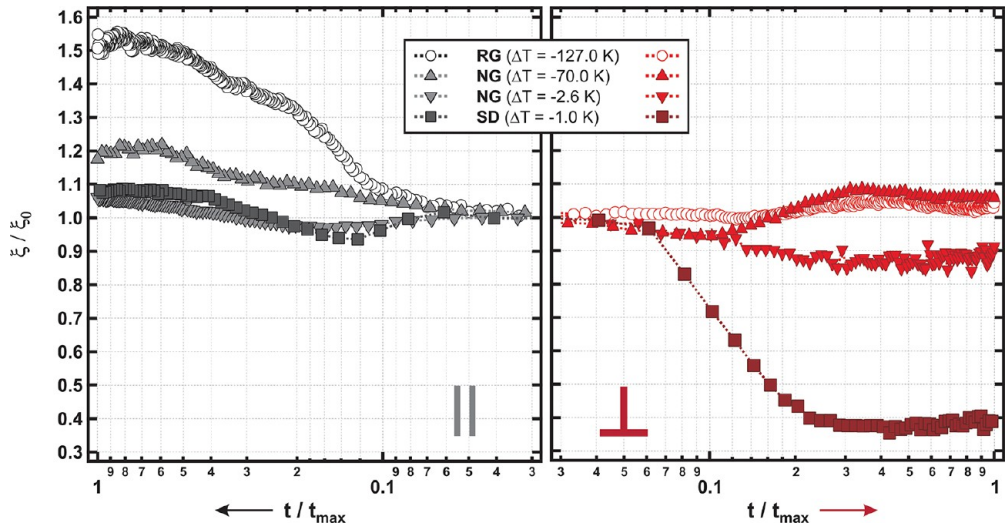

Figure 7. Normalized correlation length (ξ/ξ_0) as function of reduced lag time (t/t_{max}) upon inception of an electric field of 1 kV mm^{-1} for concentrated solutions of SI block copolymers in toluene. The characteristic time evolution of the correlation length for lamellae oriented parallel (left) and perpendicularly (right) to E indicates the dominant alignment mechanisms in the presence of an electric field: (i) RG in case of a strongly segregated lamellar phase (open circles, $S_{48}I_{52}^{80}$, $\Delta T \approx -127$ K), (ii) NG for moderately segregated blocks as illustrated for $S_{48}I_{52}^{80}$ at $\Delta T = -70$ K (up-pointing triangles) and $S_{42}I_{58}^{108}$ at $\Delta T = -2.6$ K (down-pointing triangles), (iii) SD in close vicinity to ODT where lamellae are weakly segregated as shown for $S_{42}I_{58}^{108}$ at $\Delta T = -1.0$ K (solid squares). ξ_0 denotes the initial correlation length in the absence of an applied field.

temperature window where SD is the prevalent mechanism, we evaluated the temperature dependence of the asymptotic asymmetry $(\xi_\parallel/\xi_\perp)_{max}$ (see Figure 6a). This indicator increases with temperature on approaching ODT, attains a maximum in a small window in its proximity, and eventually starts to decrease when nonselective disordering becomes dominant for temperatures sufficiently close to $T_{ODT}(E)$. As outlined above, the increase in $(\xi_\parallel/\xi_\perp)_{max}$ is caused primarily by a suppression of $\xi_\perp$. For an applied field of 1 kV mm^{-1}, $(\xi_\parallel/\xi_\perp)_{max}$ exhibits a marked transition from NG to SD 1.0 K below T_{ODT}. Higher fields enable selective disordering at lower temperatures. At 3 kV mm^{-1}, SD becomes prevalent at about 1.6 K below T_{ODT} (see Figure 6b, red shaded area).

Farther below ODT, both NG and SD concur as competing mechanisms. An example is given in Figure 4b for an applied field of 3 kV mm^{-1} at $\Delta T = -2.6$ K (left). Here, lamellar grains exceeding the critical grain size ($\xi_\perp > \xi_\perp^*$) may either completely disintegrate (SD) or enable the migration of grain boundaries to spawn new grains with lamellar planes oriented parallel to the applied field (NG). We note that ill-aligned lamellae are stable as long the grain size does not exceed the critical size, that is, as long as the condition $\xi_\perp < \xi_\perp^*$ holds.[71] Indeed, $\xi_\perp$ gradually increases following an initial decline and converges asymptotically during the later stages, implying $\xi_\perp(E) < \xi_\perp(0)$, as may well be expected in the presence of an applied field. The existence of such an intermediate regime, where both mechanisms coexist, strongly suggests a continuous transition between SD and NG (Figure 6b).

Rotation of Grains, Nucleation and Growth, and Selective Disordering: Evolution of Grain Size. The evolution of ξ in the presence of an electric field offers some insight into how an applied field affects the lamellar morphology for different degrees of segregation. Figure 7 compiles the time evolution of ξ in the presence of an applied field for all data discussed in this article. The data was normalized to the initial correlation length ξ_0 in the absence of an applied field and summarizes the situations for lyotropic solutions of $S_{48}I_{52}^{80}$, studied both under ambient conditions ($\Delta T \approx -127$ K) and at elevated temperatures ($\Delta T = -70$ K). The figure further includes the data for $S_{42}I_{58}^{108}$, which was studied in proximity to ODT (-2.6 K $\leq \Delta T \leq -0.01$ K). Figure 7 thereby covers a wide range of diblock segregation from strongly segregated domains well below ODT to the situation where chemically distinct copolymer components are merely weakly segregated. We may discriminate three situations, which are schematically illustrated in Figure 8.

In the case of strongly segregated diblocks ($\Delta T \approx -127$ K, Figure 7), the application of an electric field enables the rotation of entire grains (RG) through the migration and subsequent annihilation of disclinations and edge dislocations perpendicular to the lamellar planes (RG, Figure 8). Indeed, the mean transverse grain size of parallel aligned lamellae considerably improves during alignment and $\xi_\parallel$ substantially increases accordingly, while $\xi_\perp$ remains mostly unaffected. In an intermediate regime, where distinct copolymer domains are less strongly segregated, electric-field-induced critical undulations seed the growth of parallel-aligned lamellae through the migration of

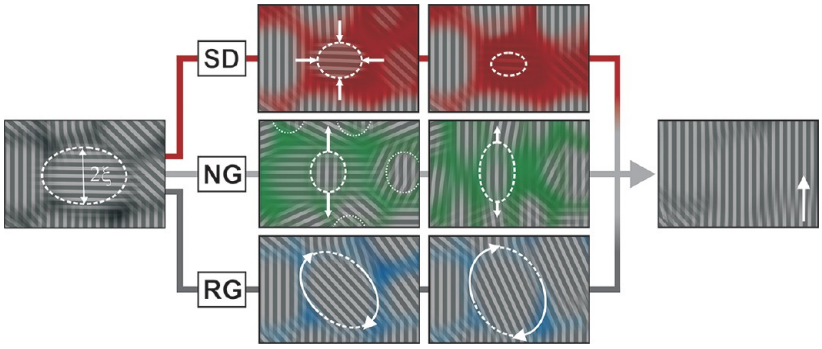

Figure 8. Schematic representation of the three distinct orientation mechanisms, which afford the alignment of block copolymer lamellae in the presence of an electric field. The minor axis of the white ellipsoids symbolizes the transverse lamellar grain dimension 2ξ. In close vicinity to ODT, alignment proceeds *via* selective disordering (SD), that is, the applied field selectively disintegrates ill-aligned lamellae, while lamellae oriented parallel to E prevail. When lamellar domains are strongly segregated, the alignment proceeds *via* the rotation of grains (RG), enabled through the migration and annihilation of defects. In an intermediate regime, buckling layer instabilities nucleate the growth of parallel aligned lamellae (NG), which proceeds through grain boundary migration. The white arrow to the right indicates the direction of E.

grain boundaries (NG, Figure 8). This inherently entails, during early and intermediate stages, the same susceptibility toward topological defects as the nucleation and growth of pristine grains in the absence of an electric field. Indeed, the time evolution of ξ barely changes when NG is the prevalent mechanism ($\Delta T = -70$ K and $\Delta T = -2.6$ K, Figure 7). We do, however, notice a slight increase in ξ irrespective of orientation at higher temperatures, which we attribute to thermal coarsening. In close vicinity to ODT ($\Delta T = -1$ K, Figure 7), the electric field selectively disintegrates perpendicular lamellae and $\xi_{\perp}$ considerably diminishes, while parallel lamellae prevail (SD, Figure 8). We refer to the literature for a more detailed discussion of outlined mechanisms.[42,44,48,72]

Nucleation and Growth *versus* Selective Disordering. The selective disintegration of lamellae in the presence of an external field may well be considered to be a subset of the NG mechanism. Ultimately, the critical grain size above which perpendicular lamellae become unstable diminishes at sufficiently high fields, as $\xi^* \sim E^{-2}$. There may thus be a situation when highly undulating lamellae of diminishing size and evanescent lamellar clusters in the disordered phase become indistinguishable both experimentally and phenomenologically. In both cases, diverging instabilities in the local composition spawn new lamellae; either composition fluctuations in the disordered phase or layer instabilities in smectic-like domains.

However, the original NG mechanism is understood to nurture the nucleation and growth of parallel lamellae by grain boundary migration, which demands the existence of physical grains over relevant time scales. To the contrary, nucleation and growth upon SD can be seen as classic nucleation from an isotropic melt. Indeed, this constitutes a decisive difference between SD and NG form a very practical point of view. Once ill-aligned grains are selectively dissolved in the presence of an electric field, the coarsening of well-aligned lamellae by consuming the disordered melt may well advance lamellar alignment even in the absence of a field. Yet, this option largely depends on the relative rates between nucleation and coarsening.

CONCLUSION

We have demonstrated how an external electric field applied close to the order−disorder transition of a block copolymer lamellar phase selectively disintegrates perpendicularly aligned lamellae, while parallel lamellae are preserved. The disintegration of ill-aligned lamellae implies the formation of a localized disordered melt, which enables the subsequent growth of parallel lamellae and thus the apparent alignment of diblock lamellae parallel to the applied field—a mechanism proposed almost two decades ago and only recently corroborated by simulations to be experimentally viable. Selective disordering scales quadratically with the dielectric contrast between chemically distinct copolymer components, which suggests that block copolymers with high dielectric contrast may exhibit a considerable selective response over a reasonable temperature and concentration range. Considering processing conditions in proximity to ODT, the application of an electric field may thus afford the selective disintegration of ill-aligned lamellae and consequently an effective way to mitigate the degree of orientational disorder. Well below ODT on the other hand, lamellar alignment proceeds through the migration and annihilation of defects which enables the rotation of grains. Our present study supports the notion that lamellar alignment through grain rotation is accompanied by a significant transverse growth of parallel-aligned lamellae. Hence, the localized application of an electric field may well complement conventional annealing techniques (*e.g.*, thermal and/or solvent vapor assisted annealing) both in proximity to the disordered phase and well below; either by diminishing orientational disorder or

mitigating the density of topological defects perpendicular to the applied field, respectively. In light of the minuscule length scales pertinent to today's process technologies, our results suggest that electric field assisted floating zone annealing may well be of some technological appeal.

METHODS AND MATERIALS

Sample Characterization. Poly(styrene-*b*-isoprene) (SI) copolymers were synthesized by sequential living anionic polymerization as detailed elsewhere.[73] Molecular weight and polydispersity were determined by gel permeation chromatography (GPC), and the composition by Nuclear Magnetic Resonance Spectroscopy (^{1}H NMR). Small-angle X-ray scattering (SAXS) confirmed a lamellar morphology at ambient temperatures in bulk and in solutions of toluene above the order−disorder concentration. Sample characteristics are summarized in Table 1.

Time-Resolved *in Situ* Small-Angle X-ray Scattering in the Presence of an Electric Field. SAXS was conducted at the European Synchrotron Radiation Facility (ESRF) in Grenoble, France, on beamline ID02 using a monochromatic beam at 12.5 keV and a spot size at the sample of 200 × 400 μm^2 (vertical and horizontal, respectively). SAXS data were recorded at a sample-to-detector distance of 5 m using the FReLoN 2D X-ray detector in high-speed mode with 4 × 4 binning, resulting in an effective resolution of 512 × 512 pixels. Instrument resolution is determined by the point-spread function of the detector's conversion phosphor, which amounts to about 80 μm and translates to an instrumental breadth of about 0.001 nm. Raw data was corrected for detector dark current and efficiency, sample absorption, and geometry, prior to normalization to transmitted beam intensity. Temperature-dependent SAXS experiments in the presence of an external electric field of $S_{42}I_{58}$[108] solutions in toluene (32.5 wt %) were conducted *in situ* utilizing a custom-built capacitor, which accommodated square quartz capillaries (2 × 2 mm^2) between parallel electrodes. Both, flame-sealed capillaries and electrodes were fully immersed in a high dielectric insulating oil that afforded the precise control of the sample temperature with accuracy better than ±0.4 K. Within the sensitivity of the setup (0.01 mA), no leakage currents were detected. The sample cell was positioned to allow the beam to illuminate the capillary's center.

Temperature-Dependent Measurements and Data Analysis. The order−disorder transition temperature (T_{ODT}) of $S_{42}I_{58}$[108] solutions was determined by ten independent heating and cooling cycles about the order−disorder transition. The average of the heating cycles was used as the transition temperature, T_{ODT} = 58.05 ± 0.43 °C. Samples were homogenized by equilibrating the solution above T_{ODT} to exhibit homogeneously isotropic correlation hole scattering distinctive for block copolymer solution in the mixed phase. Subsequently, the samples were cooled down and equilibrated at the desired sample temperature below T_{ODT} prior to applying the electric field. The scattering data presented for $S_{48}I_{52}$[80] has been published previously and we refer to the literature[48] for experimental details.

Normalized and geometry-corrected 2D scattering data were regrouped by computing the azimuthally averaged scattering intensities as a function of the scattering vector $Q = 4\pi/\lambda \sin\theta$ within wedged-shaped sectors aligned along azimuthal angles, $\varphi = 90 \pm 15°$ and $\varphi = 90 \pm 15°$, respectively, including the mirroring sectors. Here, λ denotes the wavelength of the incident beam and 2θ is the scattering angle. The peak position Q_{max} and the peak width (fwhm) were determined by a Pseudo-Voigt peak shape analysis. The fitting function employed for data analysis is provided as Supporting Information.

Conflict of Interest: The authors declare no competing financial interest.

Acknowledgment. We thank P. Boesecke and T. Narayanan for their technical assistance at ID02 and acknowledge provision of beam time by the European Synchrotron Radiation Facility (ESRF). The authors thank S. Hiltl, K. Schindler, and C. Liedel for their invaluable support during beam time. C.W.P., A.B., G.J.A.S., and K.M.L. thank the German Science Foundation (DFG, BO 2475/5-1) and the European Union for financial support in the framework of the ERA-NanoSci+ project MEMORY. M.R. and V.S.U. were supported by the U.S. Department of Energy, Basic Energy Sciences, Materials Sciences and Engineering Division.

Supporting Information Available: Details of data analysis including the fitting function employed in this study. Supporting Information also includes the time evolution of the line shape for the dominant scattering intensity for SD and NG, and the time evolution of $\xi_\perp/\xi_\parallel$ for all sampled temperatures and electric fields studied for the present paper. Further, we show the time evolution of the peak scattering intensity for the alignment of the lamellar phase of $S_{48}I_{52}$[80] at $\Delta T \approx -70$ K, which proceeds *via* NG and follows approximately the same scaling as discussed for Figure 2b. Finally, we provide movies compiling the complete set of DDFT simulation data as discussed for Figure 4. This material is available free of charge *via* the Internet at http://pubs.acs.org/.

REFERENCES AND NOTES

1. Hadjichristidis, N.; Pispas, S.; Floudas, G. *Block Copolymers: Synthetic Strategies, Physical Properties, and Applications*; John Wiley & Sons, Inc.: Hoboken, 2002; Chapter 19, pp 346−361.
2. Abetz, V.; Simon, P. Phase Behaviour and Morphologies of Block Copolymers. *Adv. Polym. Sci.* **2005**, *189*, 125–212.
3. Bang, J.; Jeong, U.; Ryu, D. Y.; Russell, T. P.; Hawker, C. J. Block Copolymer Nano-lithography: Translation of Molecular Level Control to Nanoscale Patterns. *Adv. Mater.* **2009**, *21*, 4769–4792.
4. Park, C.; Yoon, J.; Thomas, E. L. Enabling Nanotechnology with Self Assembled Block Copolymer Patterns. *Polymer* **2003**, *44*, 6725–6760.
5. Nie, Z.; Kumacheva, E. Patterning Surfaces with Functional Polymers. *Nat. Mater.* **2008**, *7*, 277–290.
6. Edwards, E.; Montague, M.; Solak, H.; Hawker, C.; Nealey, P. Precise Control over Molecular Dimensions of Block-Copolymer Domains Using the Interfacial Energy of Chemically Nanopatterned Substrates. *Adv. Mater.* **2004**, *16*, 1315–1319.
7. Cheng, J. Y.; Ross, C. A.; Smith, H. I.; Thomas, E. L. Templated Self-Assembly of Block Copolymers: Top-Down Helps Bottom-Up. *Adv. Mater.* **2006**, *18*, 2505–2521.
8. Chang, J.-B.; Son, J. G.; Hannon, A. F.; Alexander-Katz, A.; Ross, C. A.; Berggren, K. K. Aligned Sub-10-nm Block Copolymer Patterns Templated by Post Arrays. *ACS Nano* **2012**, *6*, 2071–2077.
9. Berry, B. C.; Bosse, A. W.; Douglas, J. F.; Jones, R. L.; Karim, A. Orientational Order in Block Copolymer Films Zone Annealed Below the Order-Disorder Transition Temperature. *Nano Lett.* **2007**, *7*, 2789–2794.
10. Fukunaga, K.; Elbs, H.; Magerle, R.; Krausch, G. Large-Scale Alignment of ABC Block Copolymer Microdomains *via* Solvent Vapor Treatment. *Macromolecules* **2000**, *33*, 947–953.
11. Kim, T. H.; Hwang, J.; Hwang, W. S.; Huh, J.; Kim, H.-C.; Kim, S. H.; Hong, J. M.; Thomas, E. L.; Park, C. Hierarchical Ordering of Block Copolymer Nanostructures by Solvent Annealing Combined with Controlled Dewetting. *Adv. Mater.* **2008**, *20*, 522–527.
12. Segalman, R. A.; Yokoyama, H.; Kramer, E. J. Graphoepitaxy of Spherical Domain Block Copolymer Films. *Adv. Mater.* **2001**, *13*, 1152–1155.

13. Kim, S. O.; Solak, H. H.; Stoykovich, M. P.; Ferrier, N. J.; De Pablo, J. J.; Nealey, P. F. Epitaxial Self-Assembly of Block Copolymers on Lithographically Defined Nanopatterned Substrates. *Nature* **2003**, *424*, 411–414.
14. Chen, Z. R.; Kornfield, J. A.; Smith, S. D.; Grothaus, J. T.; Satkowski, M. M. Pathways to Macroscale Order in Nanostructured Block Copolymers. *Science* **1997**, *277*, 1248–1253.
15. Angelescu, D. E.; Waller, J. H.; Adamson, D. H.; Deshpande, P.; Chou, S. Y.; Register, R. A.; Chaikin, P. M. Macroscopic Orientation of Block Copolymer Cylinders in Single-Layer Films by Shearing. *Adv. Mater.* **2004**, *16*, 1736–1740.
16. Grigorova, T.; Pispas, S.; Hadjichristidis, N. Magnetic Field Induced Orientation in Diblock Copolymers with One Crystallizable Block. *Macromolecules* **2005**, *38*, 7430–7433.
17. Tao, Y. F.; Zohar, H.; Olsen, B. D.; Segalman, R. A. Hierarchical Nanostructure Control in Rod-Coil Block Copolymers with Magnetic Fields. *Nano Lett.* **2007**, *7*, 2742–2746.
18. Mauter, M. S.; Elimelech, M.; Osuji, C. O. Nanocomposites of Vertically Aligned Single-Walled Carbon Nanotubes by Magnetic Alignment and Polymerization of a Lyotropic Precursor. *ACS Nano* **2010**, *4*, 6651–6658.
19. Majewski, P. W.; Gopinadhan, M.; Osuji, C. O. Magnetic Field Alignment of Block Copolymers and Polymer Nanocomposites: Scalable Microstructure Control in Functional Soft Materials. *J. Polym. Sci., Part B: Polym. Phys.* **2012**, *50*, 2–8.
20. Morkved, T. L.; Lu, M.; Urbas, A. M.; Ehrichs, E. E.; Jaeger, H. M.; Mansky, P.; Russell, T. P. Local Control of Microdomain Orientation in Diblock Copolymer Thin Films with Electric Fields. *Science* **1996**, *273*, 931–933.
21. Thurn-Albrecht, T.; DeRouchey, J.; Russell, T. P.; Jaeger, H. M. Overcoming Interfacial Interactions with Electric Fields. *Macromolecules* **2000**, *33*, 3250–3253.
22. Böker, A.; Elbs, H.; Hänsel, H.; Knoll, A.; Ludwigs, S.; Zettl, H.; Urban, V.; Abetz, V.; Müller, A. H. E.; Krausch, G. Microscopic Mechanisms of Electric-Field-Induced Alignment of Block Copolymer Microdomains. *Phys. Rev. Lett.* **2002**, *89*, 135502.
23. Xu, T.; Zhu, Y. Q.; Gido, S. P.; Russell, T. P. Electric Field Alignment of Symmetric Diblock Copolymer Thin Films. *Macromolecules* **2004**, *37*, 2625–2629.
24. Russell, T. P.; Mansky, P.; DeRouchey, J.; Mays, J.; Pitsikalis, M.; Morkved, T.; Jaeger, H. Large-Area Domain Alignment in Block Copolymer Thin Films Using Electric Fields. *Macromolecules* **1998**, *31*, 4399–4401.
25. Morariu, M. D.; Voicu, N. E.; Schäffer, E.; Lin, Z.; Russell, T. P.; Steiner, U. Hierarchical Structure Formation and Pattern Replication Induced by an Electric Field. *Nat. Mater.* **2003**, *2*, 48–52.
26. Olszowka, V.; Hund, M.; Kuntermann, V.; Scherdel, S.; Tsarkova, L.; Böker, A.; Krausch, G. Large Scale Alignment of a Lamellar Block Copolymer Thin Film *via* Electric Fields: A Time-Resolved SFM Study. *Soft Matter* **2006**, *2*, 1089–1094.
27. Amundson, K.; Helfand, E.; Quan, X.; Smith, S. D. Alignment of Lamellar Block Copolymer Microstructure in an Electric Field. 1. Alignment Kinetics. *Macromolecules* **1993**, *26*, 2698–2703.
28. Schmidt, K.; Schoberth, H. G.; Schubert, F.; Hänsel, H.; Fischer, F.; Weiss, T. M.; Sevink, G. J. A.; Zvelindovsky, A. V.; Böker, A.; Krausch, G. Scaling Behavior of the Reorientation Kinetics of Block Copolymers Exposed to Electric Fields. *Soft Matter* **2007**, *3*, 448–453.
29. Tsori, Y.; Tournilhac, F.; Leibler, L. Demixing in Simple Fluids Induced by Electric Field Gradients. *Nature* **2004**, *430*, 544–547.
30. Wirtz, D.; Fuller, G. G. Phase-Transitions Induced by Electric-Fields in Near-Critical Polymer-Solutions. *Phys. Rev. Lett.* **1993**, *71*, 2236–2239.
31. Xu, T.; Zvelindovsky, A. V.; Sevink, G. J. A.; Gang, O.; Ocko, B.; Zhu, Y. Q.; Gido, S. P.; Russell, T. P. Electric Field Induced Sphere-to-Cylinder Transition in Diblock Copolymer Thin Films. *Macromolecules* **2004**, *37*, 6980–6984.
32. Schoberth, H. G.; Schmidt, K.; Schindler, K. A.; Böker, A. Shifting the Order-Disorder Transition Temperature of Block Copolymer Systems with Electric Fields. *Macromolecules* **2009**, *42*, 3433–3436.
33. Schmidt, K.; Schoberth, H. G.; Ruppel, M.; Zettl, H.; Hänsel, H.; Weiss, T. M.; Urban, V.; Krausch, G.; Böker, A.; Hänsel, H. Reversible Tuning of a Block-Copolymer Nanostructure *via* Electric Fields. *Nat. Mater.* **2008**, *7*, 142–145.
34. Pester, C. W.; Ruppel, M.; Schoberth, H. G.; Schmidt, K.; Liedel, C.; van Rijn, P.; Schindler, K. A.; Hiltl, S.; Czubak, T.; Mays, J.; et al. Piezoelectric Properties of Non-Polar Block Copolymers. *Adv. Mater.* **2011**, *23*, 4047–4052.
35. Darling, S. B. Directing the Self-Assembly of Block Copolymers. *Prog. Polym. Sci.* **2007**, *32*, 1152–1204.
36. Nelson, D. R. *Defects and Geometry in Condensed Matter Physics*; Cambridge University Press: Cambridge, U.K.; 2002.
37. Hammond, M. R.; Cochran, E.; Fredrickson, G. H.; Kramer, E. J. Temperature Dependence of Order, Disorder, and Defects in Laterally Confined Diblock Copolymer Cylinder Monolayers. *Macromolecules* **2005**, *38*, 6575–6585.
38. Kleman, M.; Friedel, J. Disclinations, Dislocations, and Continuous Defects: A Reappraisal. *Rev. Mod. Phys.* **2008**, *80*, 61–115.
39. Landau, L. D.; Lifshits, E. M.; Pitaevskii, L. P. *Course of Theoretical Physics*, 2nd ed.; Pergamon Press: Oxford, 1984.
40. Tsori, Y. Colloquium: Phase Transitions in Polymers and Liquids in Electric Fields. *Rev. Mod. Phys.* **2009**, *81*, 1471–1494.
41. Schmidt, K.; Pester, C. W.; Schoberth, H. G.; Zettl, H.; Schindler, K. A.; Böker, A. Electric Field Induced Gyroid-to-Cylinder Transitions in Concentrated Diblock Copolymer Solutions. *Macromolecules* **2010**, *43*, 4268–4274.
42. Amundson, K.; Helfand, E.; Quan, X. N.; Hudson, S. D.; Smith, S. D. Alignment of Lamellar Block Copolymer Microstructure in an Electric Field. 2. Mechanisms of Alignment. *Macromolecules* **1994**, *27*, 6559–6570.
43. Gunkel, I.; Stepanow, S.; Thurn-Albrecht, T.; Trimper, S. Fluctuation Effects in the Theory of Microphase Separation of Diblock Copolymers in the Presence of an Electric Field. *Macromolecules* **2007**, *40*, 2186–2191.
44. Pinna, M.; Schreier, L.; Zvelindovsky, A. V. Mechanisms of Electric-Field-Induced Alignment of Block Copolymer Lamellae. *Soft Matter* **2009**, *5*, 970–973.
45. Sevink, G. J. A.; Pinna, M.; Langner, K. M.; Zvelindovsky, A. V. Selective Disordering of Lamella-Forming Diblock Copolymers Under an Electric Field. *Soft Matter* **2011**, *7*, 5161–5170.
46. Fredrickson, G. H.; Leibler, L. Theory of Block Copolymer Solutions—Nonselective Good Solvents. *Macromolecules* **1989**, *22*, 1238–1250.
47. Lodge, T. P.; Pan, C.; Jin, X.; Liu, Z.; Zhao, J.; Maurer, W. W.; Bates, F. S. Failure of the Dilution Approximation in Block Copolymer Solutions. *J. Polym. Sci., Part B: Polym. Phys.* **1995**, *33*, 2289–2293.
48. Böker, A.; Elbs, H.; Hänsel, H.; Knoll, A.; Ludwigs, S.; Zettl, H.; Zvelindovsky, A. V.; Sevink, G. J. A.; Urban, V.; Abetz, V.; et al. Electric Field Induced Alignment of Concentrated Block Copolymer Solutions. *Macromolecules* **2003**, *36*, 8078–8087.
49. Schmidt, K.; Böker, A.; Zettl, H.; Schubert, F.; Hänsel, H.; Fischer, F.; Weiss, T. M.; Abetz, V.; Zvelindovsky, A. V.; Sevink, G. J. A.; et al. Influence of Initial Order on the Microscopic Mechanism of Electric Field Induced Alignment of Block Copolymer Microdomains. *Langmuir* **2005**, *21*, 11974–11980.
50. Schoberth, H.; Pester, C. W.; Ruppel, M.; Urban, V. S.; Böker, A. Orientation-Dependent Order-Disorder Transition Temperatures of Block Copolymer Lamellae in Electric Fields. Manuscript submitted for publication **2013**,
51. Böker, A.; Knoll, A.; Elbs, H.; Abetz, V.; Müller, A. H. E.; Krausch, G. Large Scale Domain Alignment of a Block Copolymer from Solution Using Electric Fields. *Macromolecules* **2002**, *35*, 1319–1325.
52. Onuki, A.; Fukuda, J. Electric Field Effects and Form Birefringence in Diblock Copolymers. *Macromolecules* **1995**, *28*, 8788–8795.

53. Klug, H. P.; Alexander, L. E. *X-Ray Diffraction Procedures for Polycrystalline and Amorphous Materials*, 2nd ed.; Wiley: New York, 1974.
54. Stribeck, N. *X-Ray Scattering of Soft Matter*; Springer: Berlin, 2010.
55. Onuki, A. Interface Instability Induced by an Electric Field in Fluids. *Physica A* **1995**, *217*, 38–52.
56. De Gennes, P.-G.; Prost, J. *The Physics of Liquid Crystals*; International Series of Monographs on Physics; Clarendon Press: Oxford, 1995.
57. Matsen, M. W. Undulation Instability in Block-Copolymer Lamellae Subjected to a Perpendicular Electric Field. *Soft Matter* **2006**, *2*, 1048–1056.
58. Tsori, Y.; Andelman, D. Thin Film Diblock Copolymers in Electric Field: Transition from Perpendicular to Parallel Lamellae. *Macromolecules* **2002**, *35*, 5161–5170.
59. Hashimoto, T.; Ogawa, T.; Han, C. D. Determination of Sharpness of Order-Disorder Transition of Block Copolymers by Scattering Methods. *J. Phys. Soc. Jpn.* **1994**, *63*, 2206–2214.
60. Sakamoto, N.; Hashimoto, T. Order-Disorder Transition of Low Molecular Weight Polystyrene-*block*-Polyisoprene. 1. SAXS Analysis of Two Characteristic Temperatures. *Macromolecules* **1995**, *28*, 6825–6834.
61. Koga, T. T.; Hashimoto, T. Ultra-Small-Angle X-Ray Scattering Studies on Order-Disorder Transition in Diblock Copolymers. *J. Chem. Phys.* **1999**, *110*, 11076–11086.
62. Hamley, I. W.; Castelletto, V. Small-Angle Scattering of Block Copolymers in the Melt, Solution and Crystal States. *Prog. Polym. Sci.* **2004**, *29*, 909–948.
63. Olvera de la Cruz, M.; Sanchez, I. C. Theory of Microphase Separation in Graft and Star Copolymers. *Macromolecules* **1986**, *19*, 2501–2508.
64. Higgins, J. S.; Benoit, H. *Polymers and Neutron Scattering*; Clarendon Press: Oxford, 1997.
65. Hołyst, R. Landau-Peierls Instability, X-Ray-Diffraction Patterns, and Surface Freezing in Thin Smectic Films. *Phys. Rev. A* **1991**, *44*, 3692–3709.
66. Hashimoto, T.; Takenaka, M.; Izumitani, T. Sharp Scaled Structure Factor Observed for Late Stage Spinodal Decomposition of Polymer Mixtures. *Polym. Commun.* **1989**, *30*, 45–47.
67. Dai, H. J.; Balsara, N. P.; Garetz, B. A.; Newstein, M. C. Grain Growth and Defect Annihilation in Block Copolymers. *Phys. Rev. Lett.* **1996**, *77*, 3677–3680.
68. DeRouchey, J.; Thurn-Albrecht, T.; Russell, T. P.; Kolb, R. Block Copolymer Domain Reorientation in an Electric Field: An *in situ* Small-Angle X-ray Scattering Study. *Macromolecules* **2004**, *37*, 2538–2543.
69. Ogawa, T.; Sakamoto, N.; Hashimoto, T.; Han, C. D.; Baek, D. M. Effect of Volume Fraction on the Order-Disorder Transition in Low Molecular Weight Polystyrene-*block*-Polyisoprene Copolymers. 2. Order-Disorder Transition Temperature Determined by Small-Angle X-Ray Scattering. *Macromolecules* **1996**, *29*, 2113–2123.
70. Sakamoto, N.; Hashimoto, T.; Han, C. D.; Kim, D.; Vaidya, N. Y. Order-Order and Order-Disorder Transitions in a Polystyrene-*block*-Polyisoprene-*block*-Polystyrene Copolymer. *Macromolecules* **1997**, *30*, 1621–1632.
71. Matsen, M. W. Stability of a Block-Copolymer Lamella in a Strong Electric Fields. *Phys. Rev. Lett.* **2005**, *95*, 258302.
72. Olszowka, V.; Hund, M.; Kuntermann, V.; Scherdel, S.; Tsarkova, L.; Böker, A. Electric Field Alignment of a Block Copolymer Nanopattern: Direct Observation of the Microscopic Mechanism. *ACS Nano* **2009**, *3*, 1091–1096.
73. Schmalz, H.; Bo, A.; Lange, R.; Krausch, G. Synthesis and Properties of ABA and ABC Triblock Copolymers with Glassy (A), Elastomeric (B), and Crystalline (C) Blocks. *Macromolecules* **2001**, *34*, 8720–8729.